JACS
JOURNAL OF THE AMERICAN CHEMICAL SOCIETY

Article

pubs.acs.org/JACS

Supramolecular Assembly of Comb-like Macromolecules Induced by Chemical Reactions that Modulate the Macromolecular Interactions In Situ

Hongwei Xia,[†] Hailin Fu,[†] Yanfeng Zhang,[§] Kuo-Chih Shih,[†] Yuan Ren,[†] Murali Anuganti,[†] Mu-Ping Nieh,[†] Jianjun Cheng,*[,§] and Yao Lin*[,†,‡]

[†]Polymer Program, Institute of Materials Science and [‡]Department of Chemistry, University of Connecticut, Storrs, Connecticut 06269, United States

[§]Department of Materials Science and Engineering, University of Illinois at Urbana−Champaign, Urbana, Illinois 61801, United States

Supporting Information

ABSTRACT: Supramolecular polymerization or assembly of proteins or large macromolecular units by a homogeneous nucleation mechanism can be quite slow and require specific solution conditions. In nature, protein assembly is often regulated by molecules that modulate the electrostatic interactions of the protein subunits for various association strengths. The key to this regulation is the coupling of the assembly process with a reversible or irreversible chemical reaction that occurs within the constituent subunits. However, realizing this complex process by the rational design of synthetic molecules or macromolecules remains a challenge. Herein, we use a synthetic polypeptide-grafted comb macromolecule to demonstrate how the in situ modulation of interactions between the charged macromolecules affects their resulting supramolecular structures. The kinetics of structural formation was studied and can be described by a generalized model of nucleated polymerization containing secondary pathways. Basic thermodynamic analysis indicated the delicate role of the electrostatic interactions between the charged subunits in the reaction-induced assembly process. This approach may be applicable for assembling a variety of ionic soft matters that are amenable to chemical reactions in situ.

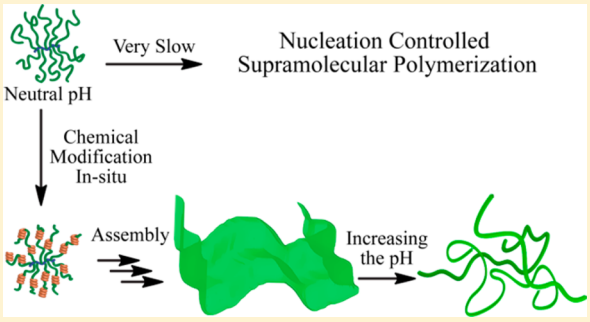

INTRODUCTION

About 50 years ago, Oosawa proposed a beautiful theoretical and experimental framework for understanding the assembly of protein molecules such as actin or flagellin molecules into large supramolecular polymers.[1−3] Since then, many more protein molecules have been found to undergo this type of supramolecular polymerization, sharing several common features.[4−17] First, there exists a critical concentration for polymerization that is related to the free energy of binding of a protein monomer to the growing edge of the protein polymer. Second, the polymerization usually consists of two processes: nucleation and growth, in analogy to crystallization phenomena or gas−liquid condensation. Third, both the monomer−polymer equilibrium and the polymerization rate may be regulated by changing the conformation of protein monomers and the monomer−monomer interactions with a chemical reaction (e.g., in the binding of ATP to actin and its subsequent hydrolysis). Inspired by the sophisticated protein polymerization mechanisms in nature, numerous synthetic or hybrid molecules have been designed to obtain a variety of supramolecular structures with interesting physical properties and functions.[18−25] The equilibrium thermodynamic and the kinetic models established from the earlier studies have markedly contributed to the rapid progress of research in the field.[8,10,26−30]

Recently, a considerable effort has been made on exploring the dynamic behaviors of supramolecular polymers to further understand the design principles of supramolecular polymers as a functional system.[31−34] As demonstrated in nature, regulation of the monomer conformation and the monomer−monomer "bonding" is a key process for dynamic behavior of protein polymers, and this can be realized by coupling the polymerization process with a reversible or irreversible chemical reaction between the monomers (Scheme 1).[3] However, realizing this type of complex processes by the rational design of synthetic molecules or macromolecules remains challenging. It is of considerable interest, both for theoretical and experimental purposes, to developing a few synthetic, minimalistic systems that can at least realize some of the protein polymerization behaviors and that are subject to in situ

Received: May 15, 2017
Published: August 4, 2017

DOI: 10.1021/jacs.7b04986
J. Am. Chem. Soc. 2017, 139, 11106−11116

Scheme 1. Polymerization of Proteins or Synthetic Subunits with a Regulation Process[a]

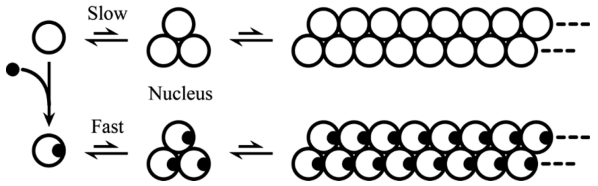

[a]e.g., by specific molecules that bind to or react with the monomers and change their interactions.

chemical modification and further regulation in aqueous solution.

We have been curious on whether polypeptide-based synthetic macromolecules may be used as a primitive yet useful model of "protein-like" subunits, for understanding the design principles of reaction-coupled polymerization or assembly processes in the artificial systems. Previously, we synthesized polypeptide-grafted comb-like macromolecules (e.g., polynorbornene-*graft*-poly(L-glutamic acids) (PN-*g*-PLGs) with a short backbone and 10−20 grafted chains), and utilized pH-tunable solubility and PLG interactions to obtain filamentous supramolecular structures in aqueous solution.[35,36] The assembly of these partially charged, comb macromolecules in solution was found to be very slow, due to the high kinetic barrier of association. This supramolecular polymerization shows distinct two-stage kinetic behavior, presumably controlled by a homogeneous nucleation mechanism.[36] Once formed, the filamentous supramolecular structures are stable in solution, possessing some of the characteristics of amyloid structures. In a later work, we presented a basic thermodynamic analysis on the filamentous assembly of partially charged subunits in solution, and related the critical concentration for polymerization to the free energy of binding of the monomers to the growing ends of supramolecular polymers.[37]

On the basis of the earlier success of this system, it is now possible to couple the assembly of the polypeptide-grafted comb macromolecules with a chemical reaction in aqueous solution, e.g., by manipulating the carboxylate groups in PLGs to modulate the conformational structures and association propensity of these grafted side chains. Carboxyl groups have been routinely utilized by nature for controlling electrostatic interactions in structural assembly. For example, the regulation of interactions between the side chain carboxyl of glutamic acids in proteins is crucial in the assembly and disassembly process of many plant viruses.[38−41] Carboxylate groups on the surface of capsid proteins, when in close proximity, can bind protons with an unusually high affinity (with a pK_a up to 7.5) and form carboxyl-carboxylate pairs (so-called "Caspar carboxylates").[5] This proton binding partially mitigates the electrostatic repulsion between the carboxylate groups to enable assembly under physiological conditions. At higher pH values, the carboxylates deprotonate and the electrostatic repulsion between neighboring carboxylates destabilizes the assembled structures, providing a trigger to elicit a biological response (e.g., the release of RNA from a virus).

Herein, using PN-*g*-PLGs as a model system, we investigate an assembly approach that utilizes a chemical reaction to neutralize a fraction of the carboxylate groups in the macromolecules in situ, and simultaneously incorporate new hydrophobic interactions between the subunits (Scheme 2). The chemical reaction modulates the secondary structure of the macromolecules and their solubility, accelerating their association. Because the assembly can take place as soon as the associative interactions become dominant, more forgiving processing conditions can be used for this assembly strategy. The reaction alters the assembly process of PN-*g*-PLGs both thermodynamically and kinetically, as evidenced in a new reaction pathway that leads to the distinct supramolecular formation of membrane structures and the accelerated rate of formation. The membrane structures are able to subsequently transform into filamentous structures by raising the pH of the solution, which enhances proton dissociation in unreacted carboxyl groups. The reaction-induced assembly process is elucidated by both the kinetic analysis based on generalized protein polymerization models, and the thermodynamic analysis that considers the competing hydrophobic and electrostatic interactions between the macromolecular subunits.

RESULTS AND DISCUSSION

Synthesis and Characterization of PN-*g*-PLGs Comb-like Macromolecules. PN_{10}-*g*-PLG_{51} and PN_{10}-*g*-PLG_{102} with a short PN backbone (DP = 10) and long PLG grafts (DP = 51 and 102) were synthesized using the method we previously reported,[35,36] their structure and composition were confirmed by gel permeation chromatography and nuclear magnetic resonance (NMR) spectroscopy (please see Figures S2−S3 and

Scheme 2. Reaction of PN-*g*-PLGs with Benzyl Amine (BA) by Using 4-(4,6-Dimethoxy-1,3,5-triazin-2-yl)-4-methyl Morpholinium Chloride (DMTMM) as the Coupling Reagent

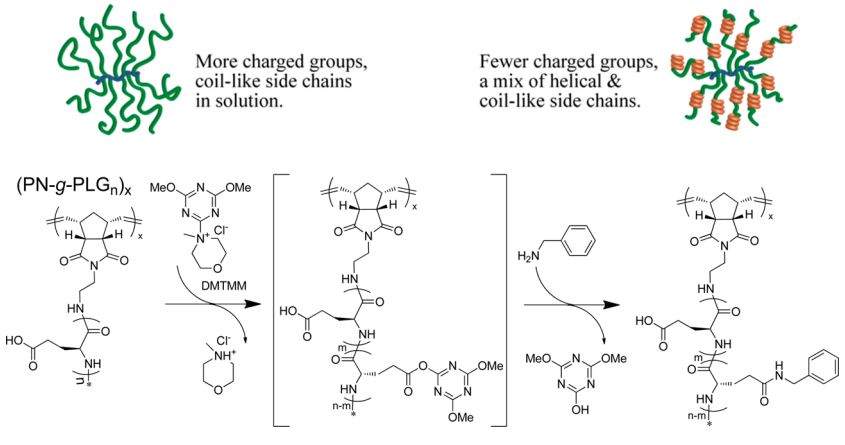

DOI: 10.1021/jacs.7b04986
J. Am. Chem. Soc. 2017, 139, 11106−11116

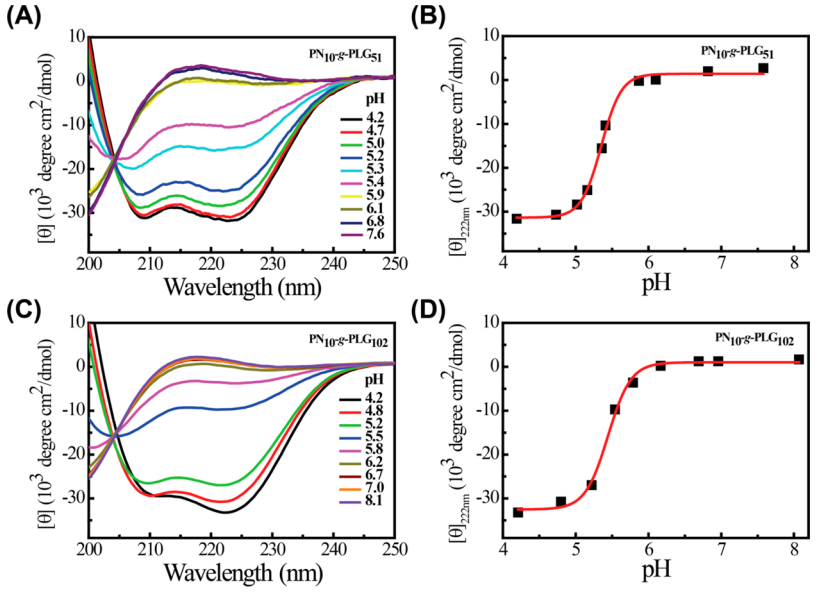

Figure 1. (A,B) Conformational changes in PN_{10}-*g*-PLG_{51} at different pHs at room temperature, as monitored by CD spectroscopy. (C,D) Conformational changes in PN_{10}-*g*-PLG_{102} at different pHs at room temperature, as monitored by CD spectroscopy. The concentration of polymers was 0.5 mg/mL. 1 M NaOH and 1 M HCl solution were used to adjust the pH, no other salts were added into the aqueous solution. The data points in (B) and (D) are fitted by a sigmoidal function (in red lines) to provide a visual guide.

Table S1 in the Supporting Information). PLGs are protonated under acidic conditions and form a helical structure.[42] When pH of the solution increases, side-chain carboxylate groups of PLGs become ionized, and PLGs extend into a coil-like conformation. The helix−coil transition is a highly cooperative process, sensitive to a small change in solution conditions. Like other polyelectrolytes, the high local concentration of carboxylate groups in PN-*g*-PLGs tends to suppress the ionization process, and causes a shift of the helix-to-coil transition to higher pH values. Therefore, the ionization and conformational profiles of these macromolecules need to be carefully determined at the chosen solution conditions. Figure 1 shows the pH dependence of the grafted polypeptide secondary structures for PN_{10}-*g*-PLG_{51} and PN_{10}-*g*-PLG_{102} macromolecules at room temperature, as monitored by circular dichroism (CD) spectroscopy. For both polymers, the onset of the helix-to-coil transition occurs near pH 4.6, and reaches completion at around pH 6.2 at RT. Previously, we demonstrated the use of the midpoint of the pH-induced helix−coil transition to induce the controlled assembly of PN-*g*-PLGs.[36] For this study, we choose pH 7, since it is well beyond the completion of helix−coil transition for these two samples. Under these solution conditions, the PLGs of the two samples form extended coils, and the macromolecules are stable against association, resulting from the charge repulsion from ionized carboxylate groups of the grafted PLGs.

The comb-like structure of PN-*g*-PLGs at pH 7 was determined by small-angle X-ray scattering (SAXS). Figure 2A shows the scattering intensity profiles $I(q)$ as a function of scattering vector q, collected from PN_{10}-*g*-PLG_{102} samples with concentrations of 4, 2, 1, and 0.5 mg/mL, respectively, in 10 mM PBS buffer (pH = 7). The scattering vector is defined as $q \equiv \frac{4\pi}{\lambda} \sin \frac{\theta}{2}$ where θ is the scattering angle and λ is the wavelength of the X-ray. Scattering patterns obtained from the four samples are nearly identical, with the intensity difference due to the sample concentration. This shows that, even at the higher concentration, PN_{10}-*g*-PLG_{102} remained in the monomeric form at pH 7; we can treat each macromolecule as an individual scattering object. The first and the second seemingly plateau regimes locate in the q range between 0.008−0.013 $Å^{-1}$ and 0.06−0.07 $Å^{-1}$ presumably correspond to the Guinier

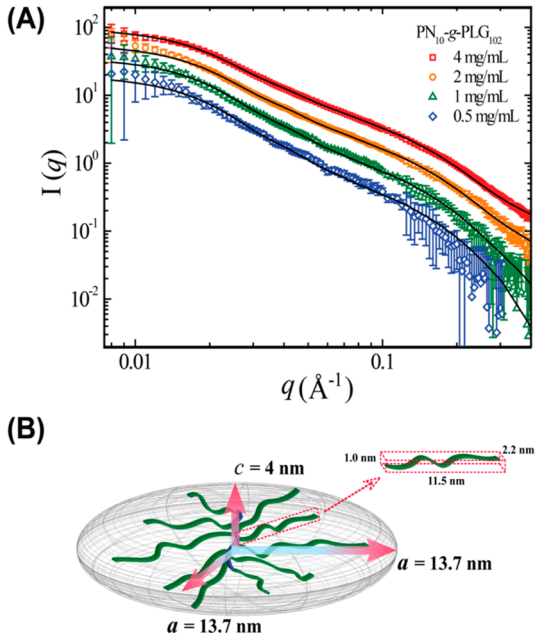

Figure 2. (A) SAXS scattering patterns from PN_{10}-*g*-PLG_{102} samples at pH 7 solution, at the concentration of 4 mg/mL (red square), 2 mg/mL (orange circle), 1 mg/mL (green triangle), and 0.5 mg/mL (blue diamond), respectively. The solid lines are the fitting results based on the model. (B) Schematic representation of a PN_{10}-*g*-PLG_{102} comb macromolecule based on the structural parameters from the model analysis, in which the scattering pattern is contributed from an oblate spheroid form factor (representing the whole PN-*g*-PLG macromolecule) and a rectangular slab form factor (representing the individual PLG chains). The PN backbone is represented by the short blue line and the grafted PLGs are represented by the long green lines.

DOI: 10.1021/jacs.7b04986
J. Am. Chem. Soc. 2017, 139, 11106−11116

region from the entire comb macromolecule and the individual grafted chain, respectively. In addition, the scattering curve follows a q^{-2} decay after the plateaus, implying relatively planar objects. As such, the scattering intensity, $I(q)$, is fit by a simple model (Figure 2B) approximated by the sum of scattering from the whole PN-*g*-PLG macromolecule (approximated as an oblate spheroid form factor) and from the individual PLG chains (approximated as a rectangular slab form factor). The equations used in the analytic procedure can be found in the experimental section in the Supporting Information. The optimized geometric parameters from the analysis are summarized in the scheme of Figure 2B. The polar (short) radius and equatorial (long) radius of the oblate PN-*g*-PLGs are 4.0 and 13.7 nm, respectively, and the dimensions of the grafted PLGs are 11.5, 2.2, and 1.0 nm in length, width and maximal thickness, respectively. The in situ SAXS results agree well with our previous ex situ TEM-based characterization[36] of such comb-like macromolecules.

To take full advantage of the electrostatic interactions from charged PN-*g*-PLGs in the regulation process, we would like to minimize the salt content of the solution. It is inevitable, however, that the ionic strength of solution may vary slightly when the reacting molecules are introduced into the solution and when the pH of solution is adjusted to the targeted range. Therefore, we further tested the stability of the PN_{10}-*g*-PLG_{102} at pH 7, with or without the presence of salts, e.g., 100 mM of NaCl. The correlation functions from the dynamic light scattering (DLS) of the samples with or without 100 mM NaCl closely match each other, indicating the stability of the macromolecular structure against the change of salt concentration (Figure S4). In both conditions, the macromolecules were well-dispersed in solution, as increasing the polymer concentrations did not change the DLS correlation function. We further tested the stability of the two polymers at different pH values. No aggregation was noticed after 24 h when the pH of the solution was maintained above 5.5 (Figure S5–6). The relative insensitivity to the bulk ionic strength in the tested conditions may be in part due to the high local molarity and proximity of carboxylate groups in the comb-like macromolecules, which may bind proton in an intricate way at this pH range.[5]

Reaction of PN-*g*-PLGs with Benzyl Amine in Solution. Synthetic polypeptides such as PLGs are particularly amenable for chemical modifications under mild conditions and make them an ideal platform for study. Scheme 2 shows our approach to modify PLG side chains in the comb macromolecules through the reaction of the carboxyl groups with amine-terminated molecules such as benzyl amine (BA). The reaction of PLGs consists of two steps: the carboxylic acids on PLGs are first activated by DMTMM, a triazine-based coupling reagent,[43] followed by the conjugation of BA to form amide. The reaction takes place at room temperature at pH 7, using DMTMM as a chemical "fuel" for the conjugation reaction. In the study, we kept the molar ratio between DMTMM and Glu as 1/1 in the reaction, and varying the ratio between BA and Glu to control the rate of the reaction and the maximal extent of amidation. We expect the BA-substitution on the side chains to reduce the charge density of the PN-*g*-PLG, affect the secondary structure of grafted chains, and enhance intermolecular association through the formation of additional hydrophobic interactions.

Figure 3 shows the reaction of PN_{10}-*g*-PLG_{102} (2 mg/mL, 13.6 mM Glu) with BA (2.9 mg/mL, 27.2 mM) and DMTMM (3.76 mg/mL, 13.6 mM) in D_2O (pH was adjusted to 7 by

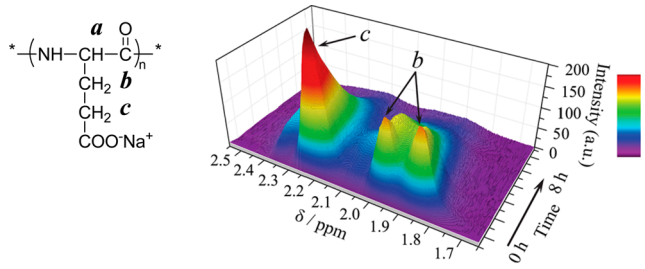

Figure 3. Time-dependent ^{1}H NMR spectra of the reaction between PN_{10}-*g*-PLG_{102} (2 mg/mL) with BA (2.91 mg/mL) in the presence of DMTMM (3.76 mg/mL) (BA/Glu/DMTMM = 2/1/1 molar ratio).

using 1 M NaOD and DCl) at RT, as monitored by ^{1}H NMR spectroscopy. As the reaction and subsequent assembly proceeds, the characteristic resonances at δ 1.6–2.5 ppm diminish, suggesting the formation an BA-substituted grafted chains and the subsequent formation of large supramolecular structures which suppress molecular motion.[44] The whole process (reaction and assembly) typically reaches completion in just a few hours at this concentration (Figure 3). As the NMR signals are affected by association of the macromolecules and require high polymer concentrations, CD spectroscopy was then used to follow the reaction-induced conformational change of PN_{10}-*g*-PLG_{102} at the lower polymer concentrations.

The transformation of carboxylic acids into amides reduces the charges in grafted PLGs and increases the local hydrophobicity, both of which should favor the formation of helical structures. We used CD spectroscopy to follow the conformational changes in situ. In the experiments, the PN_{10}-*g*-PLG_{102} concentration was kept at 0.5 mg/mL (equivalent to 3.4 mM Glu), with varying amounts of BA added into the solutions (6.8, 3.4, and 1.7 mM). After adjusting the pH of the solution back to 7, DMTMM (3.4 mM) was introduced to trigger the reaction. The time progress of the conformational changes in PN_{10}-*g*-PLG_{102} was then followed by CD spectroscopy (Figure 4). As the reaction proceeded, the conformation of the PLG segments transformed from a coil to a helical conformation. Both the rate of transformation and the maximum fraction of helicity can be modulated by the concentration of BA added into the solution. The pH of the solutions changed slightly toward the end of reaction due to the byproducts of the coupling reaction, reaching 6–6.5 for the reaction with the highest BA/Glu ratio.

To determine the final reaction yields at different conditions, the reaction products from PN_{10}-*g*-PLG_{102} with five different BA/Glu ratios (2/1, 1/1, 0.5/1, 0.2/1 and 0.1/1) in the presence of DMTMM (DMTMM/Glu was kept at 1/1) were collected after overnight incubation, extensively dialyzed against Millipore water, lyophilized, and then redispersed in D_2O by adding NaOD to make clear solution (pH 11–12) for NMR analysis (Figure 5A and Figure S8). The NMR results on the purified reaction products confirm that the BA has been introduced into the PLG side chains via the formation of amide bonds, and the substitution yields were estimated from analysis of corresponding resonance peaks. Figure 5B shows how the extent of substitution of PLGs is modulated by varying the molar ratios between BA and Glu in the reaction.

Supramolecular Assemblies from the In Situ Reaction of PN-*g*-PLGs with BA. As the reaction progressed, the reduced charges and increased hydrophobicity of grafted chains induced association of the comb macromolecules into supra-

DOI: 10.1021/jacs.7b04986
J. Am. Chem. Soc. 2017, 139, 11106–11116

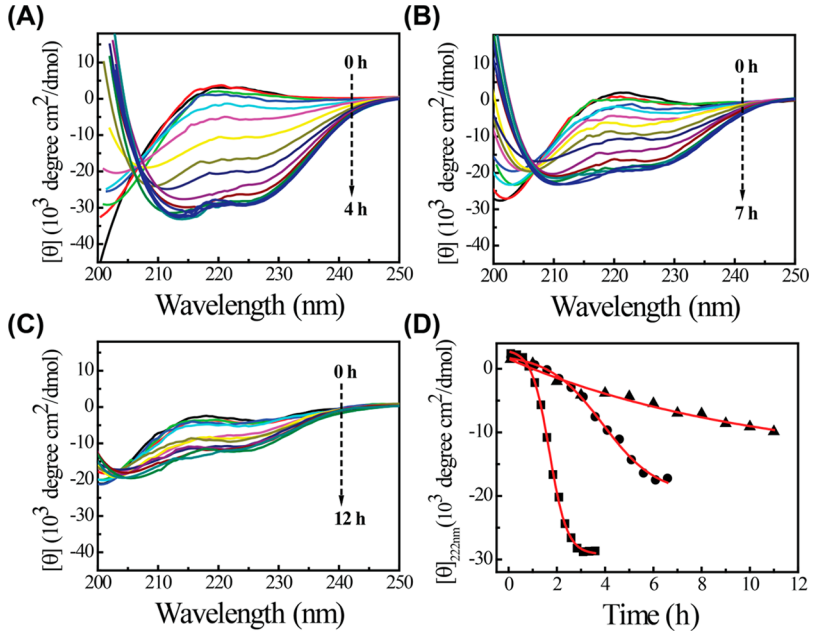

Figure 4. Time progress of the conformational changes in PLGs after PN_{10}-*g*-PLG_{102} (0.5 mg/mL, pH 7, RT) reacts with BA at the BA/Glu ratio of (A) 2/1, (B) 1/1 and (C) 0.5/1, respectively, as monitored by CD spectroscopy. (D) The kinetic profiles of the conformational changes as monitored at 222 nm, with the BA/Glu ratio of 2/1 (black squares), 1/1 (black circles) and 0.5/1 (black triangles), respectively. The data are fitted by the sigmoidal function (red lines).

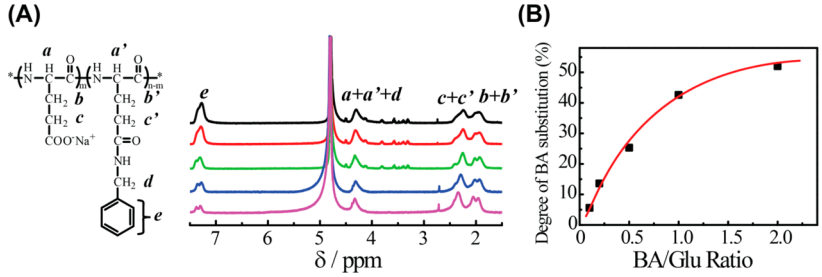

Figure 5. (A) Overlap of ^{1}H NMR spectra from the five BA-substituted PN_{10}-*g*-PLG_{102} samples in D_2O. The reaction products were obtained from overnight reactions of 0.5 mg/mL PN_{10}-*g*-PLG_{102}, with BA/Glu ratio = 2/1, 1/1, 0.5/1, 0.2/1 and 0.1/1 (from top to bottom). (B) The amidation yields of PLGs were determined from the NMR spectra in (A) and plotted against the BA/Glu ratios used in the reaction. The data are fitted by an exponential function (red line).

molecular structures. After a few hours, large assembled structures can be detected in solution by optical microscopy (Figure S9) and by confocal microscopy after staining the samples with thioflavin T (ThT) (Figure 6A–C). The supramolecular structures were examined by field emission scanning electron microscopy (FESEM) and found to form thin membrane structures (Figure 6D–F). The more extended membranes in Figure 6A and 6D have a thickness down to 13–14 nm, as measured by atomic force microscopy (AFM) (Figure S10). Interestingly, some AFM images scanned on the thinnest membranes suggest some filamentous textures (Figure S10–S11). Thin membranes seem to be formed from the association of long filaments that have the thickness of ~14 nm and varying widths (Figure S10). Increasing BA-substitution leads to membranes that are thicker and more crumpled (Figure 6C, Figure 6F and Figure S12), presumably due to the lowering of the electrostatic "tension" of the membranes and the tendency to minimize the hydrophobic patches on the surface. FTIR studies (Figure S13) on the membranes isolated from the solution indicate that the BA-substituted PN-*g*-PLGs largely adopt α-helical and coil conformation in the assemblies, in contrast to the β-sheets found previously in the assembly of unmodified PN-*g*-PLGs.[6] Recent studies have suggested that the amyloid-type, β-sheet structure may be adopted by almost any polypeptide chain, but the partition between folding and amyloid formation under the specific solution conditions depends on the relative energies of three major states: α-helix, amyloid aggregate, and random-coil.[45−47] As the reaction of PLGs with BA favors the formation of helical structures, this may therefore suppress the amyloid formation by promoting the alternative aggregation states that are kinetically more favorable compared to the β-sheets.

Interestingly, after the membranes were formed, changing the pH of the solution from 7 to 10 increases electrostatic repulsion between the macromolecular units (e.g., from unreacted Glu in the grafted chains), and facilitates the dissociation of the membrane structures into long, filamentous structures (Figure 6G–I). For the sample with a relatively low ratio of BA-substitution (BA/Glu = 0.5/1), individually dispersed, fibrous supramolecular polymers become the dominant form in the solution (Figure 6G). The diameters of the fibrous structures range from 100 to 400 nm in the images,

DOI: 10.1021/jacs.7b04986
J. Am. Chem. Soc. 2017, 139, 11106−11116

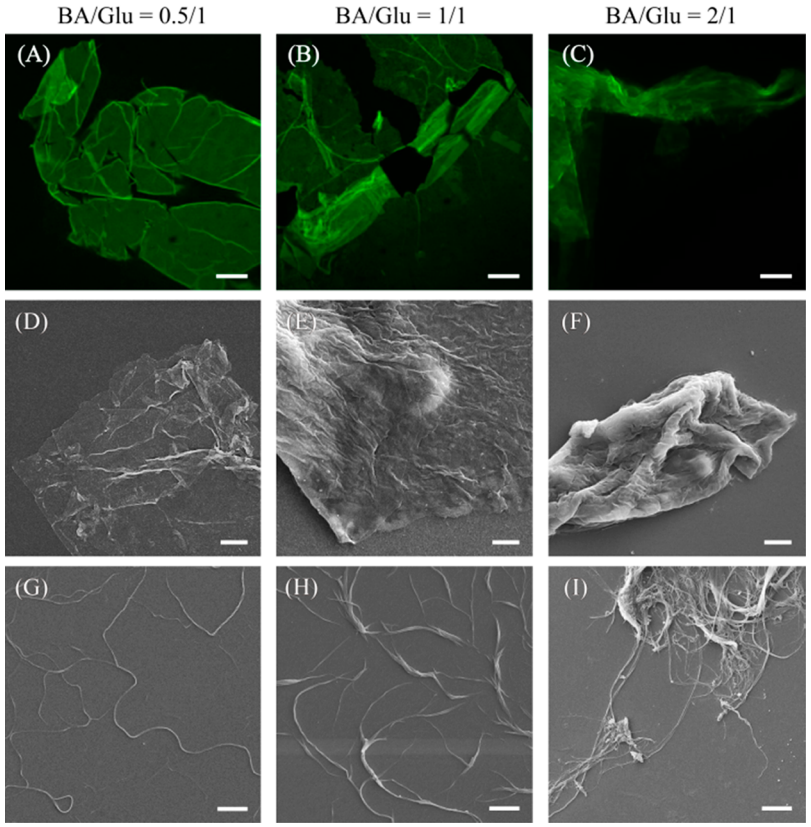

Figure 6. (A–C) Confocal microscopy images (scale bar 20 μm) stained with Thioflavin T and (D–F) FESEM images of thin membrane supramolecular structures assembled from BA substituted PN_{10}-*g*-PLG_{102} samples, with BA/Glu ratio of 0.5/1, 1/1 and 2/1 in the reaction (scale bar 2 μm). (G–I) FESEM images of fibrous supramolecular structures formed from the dissociation of the membrane structures at pH 10 (scale bar 5 μm).

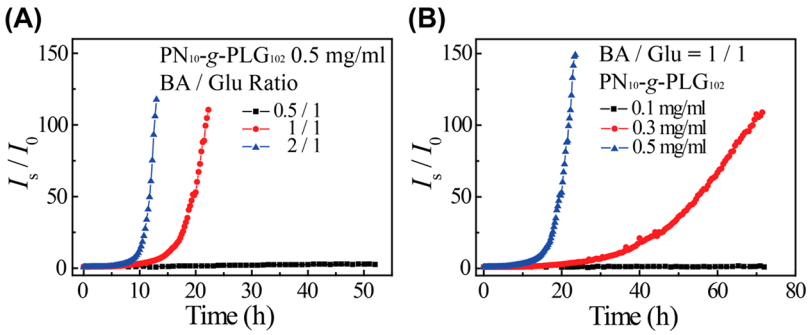

Figure 7. (A) Assembly kinetics of PN_{10}-*g*-PLG_{102} (0.5 mg/mL) with BA/Glu = 0.5/1, 1/1 and 2/1, respectively. (B) Assembly kinetics of PN_{10}-*g*-PLG_{102} concentration = 0.1 mg/mL, 0.3 and 0.5 mg/mL, respectively, with BA/Glu = 1/1, at pH 7 and RT.

with more extensive bundling and branching found in the samples with higher BA-substitution (Figure 6H–I). It suggests that the thicker membranes may also be composed of filament-like structures originally; the packing and association strengths of subunits along or among the filaments should be widely different. As such, the initial kinetic formation of supramolecular structures may indeed be dictated by the nucleation and growth of these filaments, which may follow the classic models of filamentous polymerization. Besides, the relatively weak resistance against dissociation further confirms that the assemblies of BA-substituted PN-*g*-PLGs are not amyloids in nature, which, once formed, are remarkably stable against changes of environmental conditions.

To test the general applicability of the approach, we examined the assembly behaviors of BA-substituted PN_{10}-*g*-PLG_{51} using the same reaction conditions. Similar membrane structures were found in these macromolecules (Figure S14). The reaction-induced assembly process was found to be faster in PN_{10}-*g*-PLG_{51} than that of PN_{10}-*g*-PLG_{102}. In addition, the assembly can be initiated at a range of different pHs (6–8), as the assembly would start as soon as the association becomes favorable as the reaction progresses.

Kinetic Studies on Reaction-Induced Assembly of PN-*g*-PLGs. Generally, the controlled assembly of proteins or large macromolecular units (e.g., by a nucleation–growth mechanism) can be quite slow.[2,5,7−9] In nature, the inherently slow protein polymerization (e.g., the formation of actin filaments) is often accelerated by specific regulating molecules that interact with the proteins and increase their association strengths.[9,10,14,16,48] When PN-*g*-PLGs are modified with BA,

DOI: 10.1021/jacs.7b04986
J. Am. Chem. Soc. 2017, 139, 11106–11116

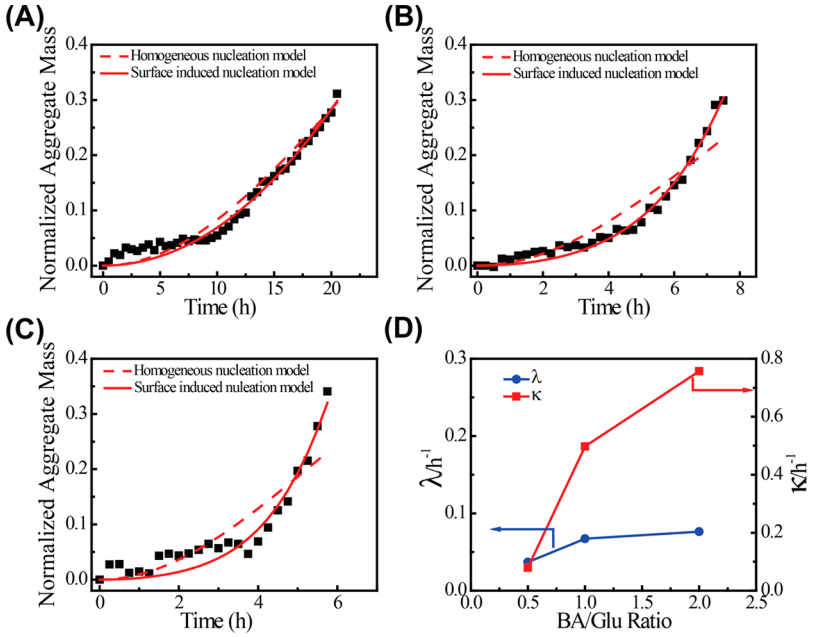

Figure 8. Model-based analysis of the assembly kinetics of PN_{10}-*g*-PLG_{102} measured by light scattering. The concentration of PN_{10}-*g*-PLG_{102} is fixed to be 0.5 mg/mL and BA/Glu ratio is varied to be (A) 0.5/1, (B) 1/1, (C) 2/1, respectively. (D) Summary of the optimized parameters based on the surface induced nucleation model.

the decrease of surface charge in the macromolecular subunits and the increase of their association strength through hydrophobic interactions should accelerate the formation of the supramolecular structures. We first studied the kinetic process of the supramolecular assembly by monitoring the scattering intensity of the solution over time using light scattering. For a given PN_{10}-*g*-PLG_{102} concentration, specific amounts of BA were added into the solution, pH adjusted, and filtered to remove dust and other impurities, after which DMTMM was introduced into the solution in order to start the conjugation reaction (DMTMM/Glu is always 1/1 molar ratio). The formation of supramolecular structures increased the intensity of scattered light and was monitored at a 90° scattering angle (Figure 7A). Increasing the BA/Glu ratio drastically accelerated the assembly process. The kinetics of reaction-induced aggregation consist of a lag phase of a few hours followed by a rapid growth phase. For a given concentration of PN_{10}-*g*-PLG_{102} (e.g., 0.5 mg/mL), we found that when the substitution was below a certain threshold (e.g., ~15% with BA/Glu = 0.2/1), no assemblies were observed within the given time frame (~48 h). On the other hand, when BA substitution was above a threshold (e.g., ~60% with BA/Glu = 5/1), phase separation was observed in the final stage. In the middle of this range, the assembly process can be well modulated by varying the molar ratios of reactants, as well as by the concentration of monomers (Figure 7B). In most of the kinetic experiments, a lag time that at least three times of what required for the reaction and the conformational changes of PLGs chains suggest there may exist a nucleation-controlled process, which is ubiquitously found in the aggregation of many native and denatured proteins and polypeptides.

A quantitative understanding of the reaction-induced assembly process is very challenging due to the evolution of the structures and association propensity of subunits by the in situ reaction, as well as the resulting heterogeneity of the system. We carried out the preliminary analysis on the kinetic profiles by focusing on whether the overall assembly process can be described by a homogeneous nucleation or a heterogeneous nucleation model. Particularly, we are curious on whether the existing models that are very successful in explaining filamentous polymerization of proteins and polypeptides may potentially be applicable to this type of complex systems in the future.

The simplest possible theory of homogeneous nucleated polymerization was the classic Oosawa model,[2,3] in which only the primary nucleation is responsible for the generation of new aggregates. On the basis of the Oosawa model, the time progress of the monomer conversion from dispersed to aggregated state ($M(t)/M_\infty$) follow a very simple form as

$$\frac{M(t)}{M_\infty} = 1 - \mathrm{Sech}^{2/n^*}\left(\lambda t\sqrt{\frac{n^*}{2}}\right) \quad (1)$$

$$\lambda = \sqrt{2k_n k_+ m_{\mathrm{tot}}{}^{n^*}} \quad (2)$$

where n^* denotes for the critical nucleus (i.e., the number of monomers in the nucleus), k_+ is the forward elongation rate constant, k_n is the primary nucleus formation rate constant, and m_{tot} denotes for the total concentration of monomers. In contrast, nucleated polymerization in the presence of secondary pathways such as surface induced nucleation follows:

$$\frac{M(t)}{M_\infty} = 1 - e^{-\left(\frac{\lambda}{\kappa}\right)^2(\cosh(\kappa t)-1)} \quad (3)$$

$$\kappa = \sqrt{2k_+ k_2 m_{\mathrm{tot}}{}^{n_2+1}} \quad (4)$$

where k_2 is the secondary nucleus formation rate constant and n_2 denotes the nucleus size of secondary nucleation process.[27,49] Approximately, λ can be considered as an effective rate constant obtained for the homogeneous nucleation process without the presence of secondary pathways, while κ being the effective rate constant that controls the secondary nucleation process.

DOI: 10.1021/jacs.7b04986
J. Am. Chem. Soc. 2017, 139, 11106−11116

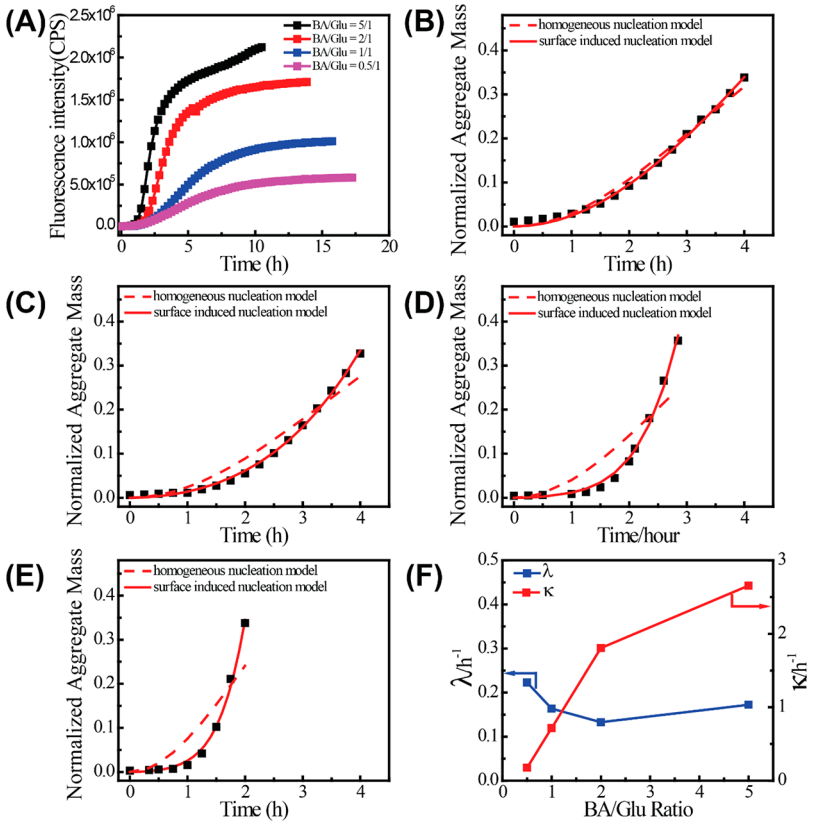

Figure 9. Model-based analysis of the assembly kinetics of PN_{10}-*g*-PLG_{51} with different BA/Glu ratios. (A) Time progress of ThT fluorescence of PN_{10}-*g*-PLG_{51} with different BA/Glu ratios. The concentration of PN_{10}-*g*-PLG_{51} is kept at 0.5 mg/mL and DMTMM/Glu is always 1/1. (B–E) Analysis of the early stage of kinetic process by the homogeneous nucleated polymerization model (in dash line) and the heterogeneous nucleated polymerization model (in solid line). BA/Glu ratio is varied as (B) 0.5/1, (C) 1/1, (D) 2/1 and (E) 5/1, respectively. (F) Summary of the obtained parameters from fitting the kinetic profiles to the surface induced nucleation model.

By first converting the changes in the light scattering intensity (Figure 7A) in the early stage to normalized aggregate mass $M(t)/M_\infty$ (see Supporting Information for the details), we can fit the experimental kinetic profiles with the two different nucleation models (eq 1 and eq 3, respectively) and obtain the corresponding parameters under each reaction condition. Figure 8A–C shows that the comparison of the best fits based on the two nucleation models, with the homogeneous nucleated polymerization model (dashed line), and the heterogeneous nucleated polymerization model in the presence of surface induced nucleation (solid line). Apparently, the early kinetic profiles found in the LS experiments are better described by the heterogeneous nucleated polymerization model. The two parameters (λ and κ) in the heterogeneous nucleation model were plotted against BA/Glu ratios in the reactions, as shown in Figure 8D. While λ varies only slightly for different reactions, κ increases rapidly with the increasing extent of substitution in the PN_{10}-*g*-PLG_{102}. By comparing eq 2 with 4, this result suggests that the secondary nucleation process was more significantly affected by the reaction than the primary nucleation, when the amidation suppresses the charges of PN-*g*-PLGs in solution. Still, the low sensitivity of light scattering in detecting the early stage of oligomer formation may be a concern. Therefore, we went on to verify our findings by examining the relatively faster kinetic behaviors of PN_{10}-*g*-PLG_{51}, using fluorescence-based methods.

The assembly kinetics of PN_{10}-*g*-PLG_{51} is faster than PN_{10}-*g*-PLG_{102} under the same reaction conditions, presumably due to the fewer charges in the macromolecules to suppress, and thereafter smaller kinetic barrier to overcome for the association between these macromolecules. We also found that the assembly process can be conveniently monitored by the introduction of ThT into solution and monitoring the large enhancement of its fluorescence emission upon binding to the assembled structures. The mechanism of ThT binding to cross-β amyloid fibrils is well studied and ThT is widely used for selectively staining and identifying amyloid fibrils.[50] More recently, its capacity to bind α-helix based structures have also been recognized.[51] By taking advantage of the ThT binding to the supramolecular structures and the large enhancement of its fluorescence, we can follow the self-assembly process with higher sensitivity than that by light scattering. Figure 9A shows the time progress of the ThT fluorescence at the wavelength of 482 nm from four different BA/Glu ratios. Figure 9B–E shows the analysis of the early stage of kinetic profiles using the heterogeneous nucleated polymerization model in the presence of surface induced nucleation (solid line). The best fitting to the profiles using homogeneous nucleated polymerization model (dashed line) are also included for comparison. The obtained parameters (λ and κ) based on eq 3 for each reaction condition are summarized in Figure 9F. The overall trend agrees well with what we found for PN_{10}-*g*-PLG_{102} based on light scattering. When the molar ratio of BA/Glu increases, κ increases monotonically, but becomes saturated when the extent of substitution on PLGs is maximized. It appears that the generalized, three-parameter heterogeneous nucleated polymerization model can reasonably describe the apparent kinetic profiles of reaction-induced assembly of PN-*g*-PLGs, which is

DOI: 10.1021/jacs.7b04986
J. Am. Chem. Soc. 2017, 139, 11106–11116

indeed a very complex and heterogeneous process. As the model was originally developed for the assembly of filamentous supramolecular polymers, the result further indicates that the formation of filaments may govern the early stage of the kinetic profiles in these systems. The strong dependence of κ on m_{tot}, as predicted by eq 4, is further investigated. In these experiments, we varied the initial concentration of PN_{10}-*g*-PLG_{51}, but kept the ratio of BA/Glu to be 5/1, which speeds up the substitution reaction to minimize the possible introduction of artificial lag phase from the reaction itself (Figure S15A). The kinetic profiles were again analyzed by the heterogeneous nucleation model (Figure S15B–E); κ obtained from the analysis is correlated with M_0 in a log–log plot (Figure S15F). A straight line is obtained, as predicted by eq 4. The slope of the line would predict a $n_2 \sim 3$, a reasonable number for the secondary nucleation process.

Our exercises above by utilizing the simple but well-established nucleated polymerization models to analyze the kinetic profiles shows a promising approach to obtain qualitative but insightful information from a highly complex system. A kinetic model that explicitly considers both the time progress of the changes in monomer properties and the nucleation and growth of the supramolecular structures is the subject of future study, which may allow for analyzing the full kinetic profiles in a quantitative manner and obtaining a deeper understanding of the interplay between different physical factors that control the reaction induced assembly process.

Thermodynamic Analysis of the Reaction-Induced Assembly Process under Competing Electrostatic and Hydrophobic Interactions. Formation of any type of assembly from identical subunits is driven by the difference in the chemical potential between the aggregated and dispersed states. A defined, self-assembled supramolecular structure usually results from a balance between short-range attractive forces (e.g., hydrogen bonds, van der Waals force, or hydrophobic interactions) and long-range repulsive forces (e.g., electrostatic interactions) of the subunits.[23,52−55] For assembly of the charged subunits in solution, the change in standard chemical potential has contributions from at least three parts: the "bond" energy in the assembly relative to separated subunits in solution, the increase of energy because of the unsaturated "bonds" from the subunits on the surface of the assembly and the electrostatic repulsion between like charges of the subunits.[37,56,57] Electrostatic repulsion can counteract the short-range attractive interactions and play an important but somewhat delicate role in the assembly; strong, dominating repulsion would prevent the association of the charged subunits while weak repulsion may lead to uncontrolled segregation in solution or even macro-phase separation. A balanced interaction depends on a number of solution parameters such as temperature, pH, ionic strength and counterions in a complex way; therefore, it is usually difficult to search through the large parameter space to find the right conditions for controlled assembly of charged subunits in aqueous solution.

The formation of membranes from BA-substituted PN-*g*-PLG is driven by the difference in the chemical potential between aggregated and dispersed states. For a given extent of reaction (α), the change in the standard chemical potential of the macromolecular subunit in an aggregate of N subunits has contributions from the stabilizing interactions between hydrophobic patches of the macromolecules, the increase of energy from the unsaturated hydrophobic patches on the rims of the membrane, and electrostatic repulsion between charged groups.[37] To calculate the nonlocal free energy associated with the screened Coulomb interaction between the subunits that make up the membrane, we may consider a large plane with uniform surface charge immersed in an electrolyte solution. Under a Debye–Hückel approximation,[52,57,58] the standard chemical potential can be expressed as

$$\Delta\mu_N^0(N, \alpha) \sim k_B T\left[-A_0\alpha\gamma + \frac{A_0\alpha\gamma}{N^{1/2}} + \sigma_0^2 A_0(1-\alpha)^2 l_B \lambda_D\right] \quad (5)$$

where A_0 is the effective contact area of each macromolecular subunit; γ is the surface tension between a hydrophobic patch and the aqueous phase, in terms of the thermal energy k_BT; σ_0 is the number (net) charge density per subunit equivalence before the substitution reaction; l_B is the Bjerrum length determining the strength of the electrostatic interactions at the conditions; λ_D is the Debye length.

Eq 5 leads to a few predictions that can be qualitatively correlated with the experiments. First, there is a critical extent of substitution (α_c), above which the free energy gained from the hydrophobic interactions of the subunits counteracts the energy cost of assembling partially charged subunits. It is also easy to show that α_c scales with $\sigma_0^2 l_B \lambda_D/\gamma$. Second, above α_c, the growth of large membranes are expected, as increasing N further decreases the mean chemical potential of subunits in the aggregates by acting on the second term of eq 5. This is evidenced in our experiments.

One can also consider the transformation of membranes into long filamentous structures upon increasing the pH of the solution. The higher pH favors the charge dissociation of unreacted Glu; the increased charge density may perturb the membranes and force the system to reconfigure to minimize free energy. The electrostatic free energy of a filament depends on how the charges are distributed (e.g., uniformly over the surface or throughout the volume) and the structures of the filament (e.g., hollow tubes or filled cylinder). For a fixed volume, the lowest energy would be found in a tubular structure with a thin wall (thickness of t) and charges distributed on both the outer (radius of r) and inner (radius of $r - t$) surfaces.[59] In an approximation, the standard chemical potential of charged subunits in such a tubular assembly can be expressed as

$$\Delta\mu_N^0(N, \alpha) \sim k_B T\left[-A_0\alpha\gamma + \frac{A_0\alpha\gamma}{N} + \sigma_0^2 A_0(1-\alpha)^2 \frac{K_0(r/\lambda_D)}{K_1(r/\lambda_D)} l_B \lambda_D\right] \quad (6)$$

where $K_n(x)$ is modified Bessel function of second kind.

The formation of tubular structures typically occurs from merging the edge of a 2-D lattice (e.g., a membrane or tape), as long as the gain of the free energy by removing the edge overcomes the excess free energy due to distortion.[3] While the tubular structures were found in the assembly of unmodified PN-*g*-PLGs previously, we do not have sufficient evidence to prove the filaments obtained in the experiments are hollow structures. Detailed structural characterization of the filaments and kinetic analysis of the transition process are the subject of future studies, which may elucidate the thermodynamic stability

DOI: 10.1021/jacs.7b04986
J. Am. Chem. Soc. 2017, 139, 11106–11116

of different supramolecular structures and the kinetic pathways for their formation.

It should also be noted that the effective contact area of the subunit A_0 depends on the topology of the macromolecules. For the same molecular weight, the comb-like macromolecular structures could have much larger A_0 than a typical Gaussian chain of polymers. Thus, the architecture of macromolecular subunits is expected to influence the assembled structures. We have tested this difference in poly(acrylic acids) and found they only form spherical or irregular aggregations after the reaction (Figure S16), rather than the membrane or filamentous structures from the comb macromolecules.

While the basic thermodynamic analysis may explain the main physical factors that governor the reaction-induced assembly process, the real situation is far more complicated, e.g., due to the heterogeneity of the reaction products and the continuing changing of association properties of the subunits under the chemical reactions. For example, if some macromolecular subunits have already been incorporated into the assembled structures before the chemical reaction completes, they may possess lower extent of substitution in comparison to the subunits that enter into the supramolecular structures later. In addition, there may exist polymorphism, as the transitions between different types of supramolecular structures may be triggered by the change of extent of reaction and other parameters. As such, the kinetic process may be intertwined with the thermodynamics and affects the final morphology and properties of the resulting supramolecular structures. Nevertheless, our approach should provide a useful way to quickly identify the extent of chemical modification that is required for controlled assembly of a specific type of subunits, under a provided environmental condition. From there, the macromolecular subunits with the optimized structures and properties can be designed and synthesized, e.g., by incorporating both ionic and nonionic amino acids into the grafted side chains in the comb polymers by random-copolymerization of amino acid *N*-carboxyanhydrides (NCAs). And for these new subunits, much higher concentration of BA may be introduced to accelerate the chemical reaction. The improved deconvolution of reaction phase from the assembly phase should provide a more reliable model system for the quantitative analysis.

CONCLUSIONS

In conclusion, we demonstrated how the in situ modulation of polypeptide interactions between the charged macromolecular subunits might affect the supramolecular structures and the kinetics of their formation. The kinetic profiles of the reaction-induced assembly may be described by existing models of surface-induced nucleated polymerization. Basic thermodynamic analysis indicates the delicate role of the electrostatic interactions between the charged subunits in the reaction-induced assembly process. This concept may be applicable to a variety of polyelectrolyte-based macromolecules or ionic nanoparticles that are amenable to surface reactions in situ. Future studies in this direction may eventually allow for a regulation mechanism by coupling a supramolecular assembly process with a chemical reaction that in situ enhances the interactions between the subunits for a controlled assembly process.

ASSOCIATED CONTENT

Supporting Information

The Supporting Information is available free of charge on the ACS Publications website at DOI: 10.1021/jacs.7b04986.

Experimental section including material synthesis, experimental procedures, and characterization data (PDF)

AUTHOR INFORMATION

Corresponding Authors

*jianjunc@illinois.edu

*yao.lin@uconn.edu

ORCID

Mu-Ping Nieh: 0000-0002-2010-8874

Jianjun Cheng: 0000-0003-2561-9291

Yao Lin: 0000-0001-5227-2663

Notes

The authors declare no competing financial interest.

ACKNOWLEDGMENTS

The research was supported by the US National Science Foundation (DMR-1150742 and CHE-1410581 to Y.L. and CHE-1308485 to J.C.). We would like to thank Dr. Ryan Baumgartner for helpful comments on the manuscript.

REFERENCES

(1) Oosawa, F.; Asakura, S.; Hotta, K.; Imai, N.; Ooi, T. *J. Polym. Sci.* **1959**, *37*, 323.

(2) Oosawa, F.; Kasai, M. *J. Mol. Biol.* **1962**, *4*, 10.

(3) Oosawa, F. *Thermodynamics of the Polymerization of Protein*; Academic Press: London, U.K., 1975.

(4) Oosawa, F. *Biophys. Chem.* **1993**, *47*, 101.

(5) Caspar, D. L. D. *Adv. Protein Chem.* **1964**, *18*, 37.

(6) Wisniewski, T.; Ghiso, J.; Frangione, B. *Biochem. Biophys. Res. Commun.* **1991**, *179*, 1247.

(7) Frieden, C. *Annu. Rev. Biophys. Biophys. Chem.* **1985**, *14*, 189.

(8) Sept, D.; McCammon, J. A. *Biophys. J.* **2001**, *81*, 667.

(9) Wegner, A. *J. Mol. Biol.* **1976**, *108*, 139.

(10) Flyvbjerg, H.; Jobs, E.; Leibler, S. *Proc. Natl. Acad. Sci. U. S. A.* **1996**, *93*, 5975.

(11) Ferrone, F. A.; Hofrichter, J.; Eaton, W. A. *J. Mol. Biol.* **1985**, *183*, 611.

(12) Asakura, S.; Eguchi, G.; Iino, T. *J. Mol. Biol.* **1964**, *10*, 42.

(13) Borisy, G. G.; Klugman, R. A.; Olmsted, J. B. *Proc. Natl. Acad. Sci. U. S. A.* **1972**, *69*, 2890.

(14) Carlier, M. F.; Pantaloni, D.; Korn, E. D. *J. Biol. Chem.* **1984**, *259*, 9983.

(15) Mitchison, T.; Kirschner, M. *Nature* **1984**, *312*, 232.

(16) Mitchison, T.; Kirschner, M. *Nature* **1984**, *312*, 237.

(17) Chen, S. M.; Ferrone, F. A.; Wetzel, R. *Proc. Natl. Acad. Sci. U. S. A.* **2002**, *99*, 11884.

(18) Tantakitti, F.; Boekhoven, J.; Wang, X.; Kazantsev, R. V.; Yu, T.; Li, J.; Zhuang, E.; Zandi, R.; Ortony, J. H.; Newcomb, C. J.; Palmer, L. C.; Shekhawat, G. S.; de la Cruz, M. O.; Schatz, G. C.; Stupp, S. I. *Nat. Mater.* **2016**, *15*, 469.

(19) Whitesides, G.; Mathias, J.; Seto, C. *Science* **1991**, *254*, 1312.

(20) De Greef, T. F. A.; Smulders, M. M. J.; Wolffs, M.; Schenning, A. P. H. J.; Sijbesma, R. P.; Meijer, E. W. *Chem. Rev.* **2009**, *109*, 5687.

(21) Aida, T.; Meijer, E. W.; Stupp, S. I. *Science* **2012**, *335*, 813.

(22) Xia, Y.; Nguyen, T. D.; Yang, M.; Lee, B.; Santos, A.; Podsiadlo, P.; Tang, Z.; Glotzer, S. C.; Kotov, N. A. *Nat. Nanotechnol.* **2011**, *6*, 580.

(23) Palmer, L. C.; Leung, C.-Y.; Kewalramani, S.; Kumthekar, R.; Newcomb, C. J.; Olvera de la Cruz, M.; Bedzyk, M. J.; Stupp, S. I. *J. Am. Chem. Soc.* **2014**, *136*, 14377.

DOI: 10.1021/jacs.7b04986
J. Am. Chem. Soc. 2017, 139, 11106−11116

(24) Yeates, T. O.; Padilla, J. E. *Curr. Opin. Struct. Biol.* **2002**, *12*, 464.
(25) Lehn, J. M. *Proc. Natl. Acad. Sci. U. S. A.* **2002**, *99*, 4763.
(26) Zhao, D.; Moore, J. S. *Org. Biomol. Chem.* **2003**, *1*, 3471.
(27) Bishop, M. F.; Ferrone, F. A. *Biophys. J.* **1984**, *46*, 631.
(28) Ferrone, F. *Methods Enzymol.* **1999**, *309*, 256.
(29) Goldstein, R. F.; Stryer, L. *Biophys. J.* **1986**, *50*, 583.
(30) Michaels, T. C. T.; Dear, A. J.; Knowles, T. P. J. *Int. Rev. Phys. Chem.* **2016**, *35*, 679.
(31) Li, X.; Kuang, Y.; Lin, H.-C.; Gao, Y.; Shi, J.; Xu, B. *Angew. Chem., Int. Ed.* **2011**, *50*, 9365.
(32) Boekhoven, J.; Brizard, A. M.; Kowlgi, K. N. K.; Koper, G. J. M.; Eelkema, R.; van Esch, J. H. *Angew. Chem., Int. Ed.* **2010**, *49*, 4825.
(33) Boekhoven, J.; Hendriksen, W. E.; Koper, G. J. M.; Eelkema, R.; van Esch, J. H. *Science* **2015**, *349*, 1075.
(34) Yu, Z.; Tantakitti, F.; Yu, T.; Palmer, L. C.; Schatz, G. C.; Stupp, S. I. *Science* **2016**, *351*, 497.
(35) Lu, H.; Wang, J.; Lin, Y.; Cheng, J. *J. Am. Chem. Soc.* **2009**, *131*, 13582.
(36) Wang, J.; Lu, H.; Kamat, R.; Pingali, S. V.; Urban, V. S.; Cheng, J.; Lin, Y. *J. Am. Chem. Soc.* **2011**, *133*, 12906.
(37) Wang, J.; Xia, H.; Zhang, Y.; Lu, H.; Kamat, R.; Dobrynin, A. V.; Cheng, J.; Lin, Y. *J. Am. Chem. Soc.* **2013**, *135*, 11417.
(38) Stubbs, G. *Philos. Trans. R. Soc., B* **1999**, *354*, 551.
(39) Wang, H.; Planchart, A.; Stubbs, G. *Biophys. J.* **1998**, *74*, 633.
(40) Ceres, P.; Zlotnick, A. *Biochemistry* **2002**, *41*, 11525.
(41) Bancroft, J. B. *Adv. Virus Res.* **1970**, *16*, 99.
(42) Myer, Y. P. *Macromolecules* **1969**, *2*, 624.
(43) Kunishima, M.; Kawachi, C.; Monta, J.; Terao, K.; Iwasaki, F.; Tani, S. *Tetrahedron* **1999**, *55*, 13159.
(44) Nakayama, M.; Okano, T. *Macromolecules* **2008**, *41*, 504.
(45) Calamai, M.; Chiti, F.; Dobson, C. M. *Biophys. J.* **2005**, *89*, 4201.
(46) Fandrich, M.; Dobson, C. M. *EMBO J.* **2002**, *21*, 5682.
(47) Baskakov, I. V.; Legname, G.; Prusiner, S. B.; Cohen, F. E. *J. Biol. Chem.* **2001**, *276*, 19687.
(48) Sept, D.; Baker, N.; Holst, M.; McCammon, J. A. *Biophys. J.* **2001**, *80*, 99A.
(49) Michaels, T. C. T.; Knowles, T. P. J. *Am. J. Phys.* **2014**, *82*, 476.
(50) Naiki, H.; Higuchi, K.; Hosokawa, M.; Takeda, T. *Anal. Biochem.* **1989**, *177*, 244.
(51) Biancalana, M.; Koide, S. *Biochim. Biophys. Acta, Proteins Proteomics* **2010**, *1804*, 1405.
(52) Israelachivili, J. *Intermolecular and Surface Forces*, 3rd ed.; Academic Press: Waltham, MA, 2011.
(53) Verwey, E. J. W. O. J. T. G. *Theory of Stability of Lypophobic Colloids*; Dover Press: Minneola, NY, 1999.
(54) Sadtler, B.; Wei, A. *Chem. Commun.* **2002**, 1604.
(55) Tomba, G.; Stengel, M.; Schneider, W.-D.; Baldereschi, A.; De Vita, A. *ACS Nano* **2010**, *4*, 7545.
(56) Oosawa, F. *J. Polym. Sci.* **1957**, *26*, 29.
(57) Kegel, W. K.; van der Schoot, P. *Biophys. J.* **2004**, *86*, 3905.
(58) Coh, E. J.; Edsall, J. T. *Proteins, Amino Acids and Peptides*; Reinhold Publishing Corp.: New York, NY, 1943.
(59) Hill, T. L. *Arch. Biochem. Biophys.* **1955**, *57*, 229.

DOI: 10.1021/jacs.7b04986
J. Am. Chem. Soc. 2017, 139, 11106−11116